Mon. Not. R. Astron. Soc. **387,** 308–318 (2008) doi:10.1111/j.1365-2966.2008.13220.x

# IPHAS discoveries of young stars towards Cyg OB2 and its southern periphery

Jorick S. Vink,[1,2⋆] Janet E. Drew,[2,3] Danny Steeghs,[4,5] Nick J. Wright,[6] Eduardo L. Martin,[7,8] Boris T. Gänsicke,[4] Robert Greimel[9,10] and Jeremy Drake[5]

[1]*Armagh Observatory, College Hill, Armagh BT61 9DG*
[2]*Imperial College of Science, Technology and Medicine, Blackett Laboratory, Exhibition Road, London SW7 2AZ*
[3]*Centre for Astrophysics Research, University of Hertfordshire, College Lane, Hatfield AL10 9AB*
[4]*Department of Physics, University of Warwick, Coventry CV4 7AL*
[5]*Harvard–Smithsonian Center for Astrophysics, 60 Garden Street, Cambridge, MA 02138, USA*
[6]*University College London, Department of Physics & Astronomy, Gower Street, London WC1E 6BT*
[7]*Instituto de Astrofisica de Canarias, 38200 La Laguna, Tenerife, Spain*
[8]*Physics Department, University of Central Florida, Orlando, FL 32816, USA*
[9]*Isaac Newton Group of Telescopes, Apartado de correos 321, E-38700 Santa Cruz de la Palma, Tenerife, Spain*
[10]*Institut für Physik, Karl-Franzen Universität Graz, Universitätsplatz 5, 8010 Graz, Austria*

Accepted 2008 March 12. Received 2008 February 15; in original form 2008 January 16

**ABSTRACT**

We report on the discovery of over 50 strong H$\alpha$ emitting objects towards the large OB association Cyg OB2 and the H II region DR 15 on its southern periphery. This was achieved using the INT Photometric H$\alpha$ Survey of the Northern Galactic Plane (IPHAS), combined with follow-up spectroscopy using the MMT multi-object spectrometer HectoSpec. We present optical spectra, supplemented with optical $r'$, $i'$ and $H\alpha$ photometry from IPHAS, and near-infrared $J$, $H$ and $K$ photometry from Two Micron All Sky Survey. The position of the objects in the $(J-H)$ versus $(H-K)$ diagram strongly suggests most of them are young. Many show Ca II infrared triplet emission indicating that they are in a pre-main-sequence phase of evolution of T Tauri and Herbig Ae nature. Among these, we have uncovered pronounced clustering of T Tauri stars roughly a degree south of the centre of Cyg OB2, in an arc close to the H II region DR 15, and the radio ring nebula G79.29+0.46, for which we discuss its candidacy as a luminous blue variable. The emission-line objects towards Cyg OB2 itself could be the brightest most prominent component of a population of lower mass pre-main-sequence stars that has yet to be uncovered. Finally, we discuss the nature of the ongoing star formation in Cyg OB2 and the possibility that the central OB stars have triggered star formation in the periphery.

**Key words:** stars: early-type – stars: emission line, Be – stars: formation – stars: individual: T Tauri – stars: pre-main-sequence.

## 1 INTRODUCTION

Cygnus OB2, with an age in the range of 1–4 Myr has been proposed to consist of approximately 2600 OB stars, including 120 O stars (Knödlseder 2000). With a total mass up to $10^5\,M_\odot$, Knödlseder (2000) argued it might be a young globular cluster in the plane of the Milky Way, although both its relatively large spatial scale (some 30 pc), and its mass (Hanson 2003), are likely to prevent it from being a true Galactic analogue of the superstar clusters found in extragalactic systems such as M82 (Smith & Gallagher 2001) and M51 (Bastian et al. 2005). Nonetheless, with a mass of the order of $10^4\,M_\odot$ (e.g. Hanson 2003), it offers, along with the Arches and Quintuplet clusters in the Galactic Centre (e.g. Figer, McLean & Morris 1999), NGC 3603 (Stolte et al. 2006), and the massive cluster Westerlund 1 (Clark et al. 2005), the best insight into the dominant mode of (massive) star formation in the Universe. It is undoubtedly the most massive OB association accessible from the Northern hemisphere, and has been discussed in the literature since the seminal study by Reddish, Lawrence & Pratt (1966). As a key feature within the highly complex Cygnus-X region (Wendker 1984; Odenwald & Schwartz 1993), it is noteworthy that its extent and distance remain controversial (cf. Comeron, Fernandez & Baraffe 2002 versus Hanson 2003).

At a distance of not less than 1.2 kpc (Hanson 2003) and probably no further than ∼1.7 kpc (e.g. Torres-Dodgen et al. 1991),

⋆E-mail: jsv@arm.ac.uk

Cyg OB2 offers the opportunity for optical studies of star formation as a function of stellar mass in a very massive cluster. Many years ago, one of the differences between low- and high-mass star formation was believed to be that the two processes occurred in very different regions. T associations, such as Taurus, were thought to be the dominant birth sites for low-mass (T Tauri) stars, while OB associations were supposed to be the nurseries for massive stars. This picture is no longer widely held. Many low-mass young stars are found in exactly the same regions as the massive OB stars (e.g. Pozzo et al. 2003; Arias et al. 2007), and observations of the proplyds in Orion (O'dell et al. 1993) suggest that the ultraviolet (UV) radiation from massive stars may evaporate the accretion discs around the low-mass stars, which may modify the initial mass function (e.g. Robberto et al. 2004).

To date, most pre-main-sequence (PMS) stars of T Tauri and Herbig type we know are found in relatively low total-mass low-concentration star-forming regions within Gould's Belt. In comparison, we lack the full picture of star formation in denser, more extreme environments within our own Galaxy where, nevertheless, the opportunity to probe deeply and at fine spatial scales is opening up. Finding these PMS stars, via their telltale H$\alpha$ emission, in a diverse range of clusters across the Galactic plane is one of the opportunities provided by the INT Photometric H$\alpha$ Survey of the Northern Galactic Plane: the IPHAS survey (Drew et al. 2005).

Here we present spectroscopic follow-up of candidate H$\alpha$-emitting point sources in the centre and to the south of Cyg OB2. In so doing, we report the first discoveries of T Tauri and Herbig Ae stars in such a massive OB association. We also identify what are most plausibly young stars that have formed in association with DR 15, the H II region to the south, first picked out at radio wavelengths by Downes & Rinehart (1966). The distance to DR 15 is commonly quoted as $\sim$1 kpc (e.g. Wendker et al. 1991). In Section 2, we describe the spectroscopic observations, and summarize the photometric IPHAS observations that prompted them. The spectroscopic, optical and near-infrared (NIR) photometric data are presented in Section 3, followed by a discussion in Section 4.

## 2 OBSERVATIONS

### 2.1 Spectroscopy: MMT/HectoSpec

The spectra presented in this paper were obtained as part of a HectoSpec programme of observations aimed at giving an in-depth characterization of the $(r' - \mathrm{H}\alpha, r' - i')$ plane that is defined by the IPHAS survey (Steeghs et al., in preparation, see also Drew et al. 2005). In this programme high priority was given to selecting relative outliers in the IPHAS colour–colour plane, with the result that nearly all high probability candidate emission-line objects within the sampled areas, in the magnitude range $17 < r' < 20$, have now been followed up spectroscopically. We refer the reader to section 6 in Drew et al. (2005) for more details on the target selection procedure.

Spectra were obtained in either 2004 June or 2005 July using the multi-object spectrograph HectoSpec mounted on the Mount Hopkins 6.5-m MMT telescope in the F/5 configuration. HectoSpec offers 300 fibres across a 1° diameter field (Fabricant et al. 2005). We used the 270 groove mm$^{-1}$ grating, which yields a wavelength range from $\sim$4500 to 9100 Å at a resolution of 6.2 Å. The total on-source exposure times were 1200 s (2004 June) and 2400 s (2005 July).

The spectra were extracted using baseline products from the HectoSpec instrument pipeline (Fabricant et al. 2005) in combination with customised sky subtraction and flux calibration tailored for our needs (Steeghs et al., in preparation). For each target, background sky information is provided by a collection of sky fibres across the field of view as well as a nearby sky measurement with the same fibre through the use of an offset exposure. Corrections for telluric absorption have been made, and a rough relative flux calibration has been applied to the spectra of targets in two of the five fields observed (Fields C and S, see below). In the 2004 June data, the sky subtraction was not always perfect because of rapid spatial variations in the diffuse and night-sky background across the field of view (see also Herbig & Dahm 2001). Hence all seeming H$\alpha$ emitters were checked carefully in order to eliminate marginal cases where incomplete sky subtraction may have created false positives. The longer 2005 July observations (in Field S), are of higher quality and hence permit a lower acceptance threshold in terms of H$\alpha$ net emission equivalent width (EW).

Here we present spectra from the five separate pointings observed that we label according to their location with respect to the notional centre of the large OB association Cyg OB2 – the position of the trapezium of bright O stars Cyg OB2 No. 8. These pointings are, respectively, C, overlapping the centre; S, immediately to the south; and Ea, Eb and Ec, in order of increasing right ascension (RA), stepping away from the association (Table 1). The region is known to be subject to significant and locally variable extinction – in Cyg OB2 itself it ranges from $A_V$ of about 3 up to over $\sim$10 (Massey & Thompson 1991; Hanson 2003; Albacete Colombo et al. 2007).

The HectoSpec observations of Fields C and S have resulted in the discovery of, respectively, 10 and 38 faint ($r' > 17$) line-emitting objects. To be directly associated with Cyg OB2 these will need to be at distances exceeding 1 kpc. In the outlying Ea field and more separated Eb and Ec fields, only a handful of analogous objects is found. We shall show below that the majority of these emission-line stars are most likely PMS objects. The locations of the major groupings in Fields C and S are marked on the image of the Cyg OB2 environment, derived from the IPHAS data base, which is shown in Fig. 1. The H$\alpha$ emitters are found both scattered around the centre of the OB association and in a striking cluster of $\sim$25 objects about 1° to the south (in the southern portion of Field S), near the position of DR 15.

### 2.2 IPHAS photometry

The photometric $r', i'$ and H$\alpha$ magnitudes presented here are all taken from the IPHAS survey (Drew et al. 2005; Gonzalez-Solares et al. 2008). Owing to reduced and variable transmission at the first attempt to image the Cyg OB2 area in the summer–autumn of 2003, repeat observations were made during the moonless and photometric nights of 2004 August 9 and 10. These later, superior data form the basis for the discussion of photometry here, and they were also employed as the basis for the selection of HectoSpec targets (Field S) for the 2005 July MMT run. For Fields C, Ea, Eb and Ec the earlier

**Table 1.** Equatorial and Galactic coordinates of the HectoSpec pointings.

| Field | RA (2000) | Dec. (2000) | $\ell$ (2000) | $b$ (2000) |
|---|---|---|---|---|
| C | 20:32:25 | +41:27:41 | 80.25 | +1.00 |
| S | 20:32:12 | +40:33:40 | 79.50 | +0.50 |
| Ea | 20:36:29 | +41:53:36 | 81.05 | +0.65 |
| Eb | 20:40:13 | +41:29:15 | 81.15 | −0.15 |
| Ec | 20:46:30 | +41:28:50 | 81.87 | −1.08 |

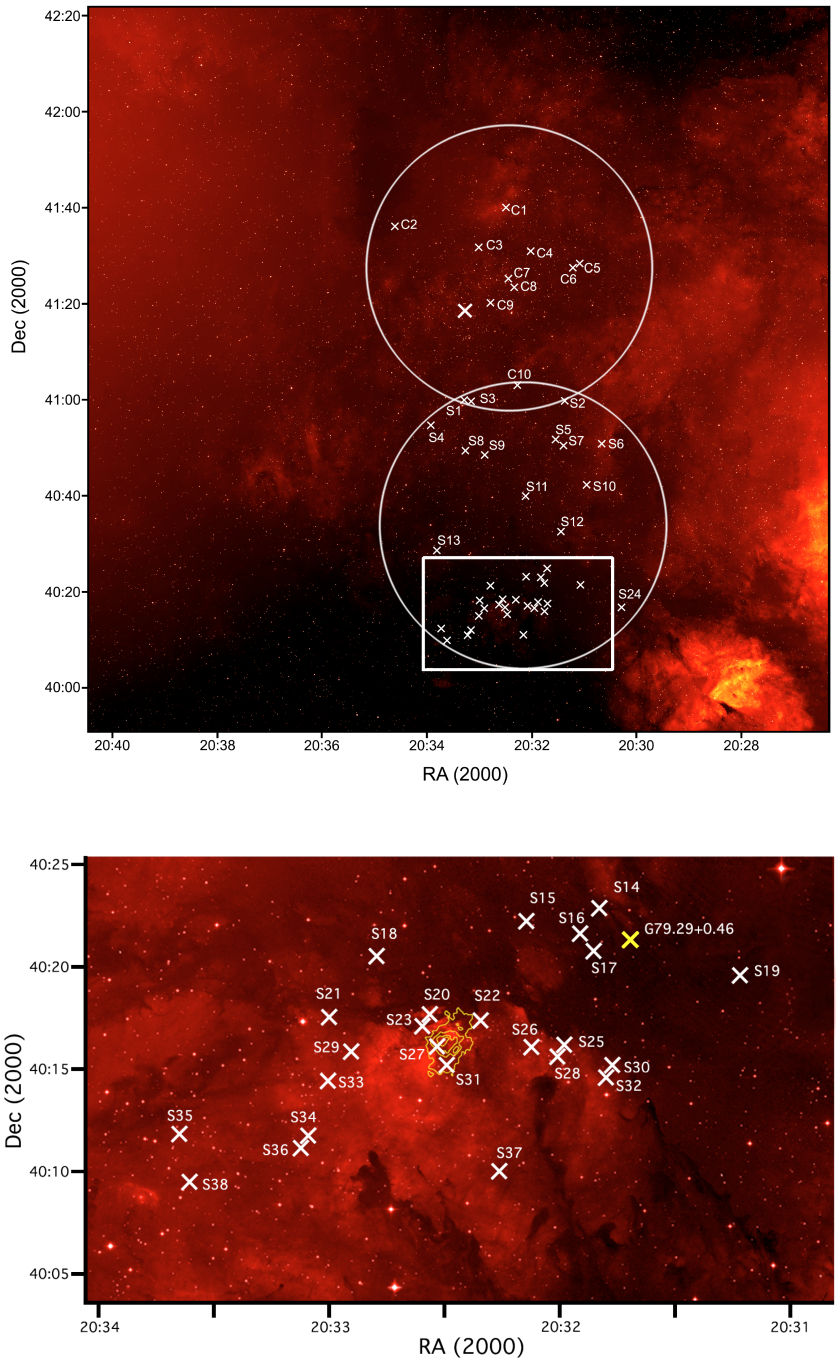


**Figure 1.** A merged IPHAS H$\alpha$ image of the sky around the centre of Cyg OB2 (the position of the trapezium of bright O stars Cyg OB2 No. 8, as indicated with a larger cross). The field of view includes the locations of the confirmed line-emitting objects from HectoSpec pointings C (upper circle) and S (lower circle). The (few) objects from pointings Ea, Eb and Ec are not plotted as they fall beyond the eastern boundary of the image. North is up, and east is towards the left-hand side. The lower figure is an enlarged area that is represented by the rectangular box in the upper figure. Note that the positions of the H II region DR 15 and the LBV candidate G79.29+0.46 are also indicated with contours and a cross, respectively.

2003 data were the only option at the time the target selections were made.

We can also utilize the repeat observations to check for emission-line variability of objects in this part of the sky. One object of particular interest is G79.29+0.46, a candidate luminous blue variable (LBV). We comment on this object and its evolutionary status in Section 3.2.3.

## 3 RESULTS

The emission-line objects we have found in Fields C and S are listed in Tables 2 and 3 and are plotted in the IPHAS colour–colour plane, shown in Figs 2 and 5. The additional six emission-line objects from Fields Ea, Eb and Ec are listed in Table 6. The tables give the $r'$ magnitudes and $(r' - i')$, $(r' - \mathrm{H}\alpha)$ colours, derived from

**Table 2.** Positions and magnitudes for the emission-line stars in the central Field C. The $r'$ magnitudes and $(r' - i')$, $(r' - \mathrm{H}\alpha)$ colours have been taken from the best IPHAS imaging (obtained in 2004 August). The H$\alpha$ EWs quoted in the final column are indicative only ($\pm$10 per cent), as the pipeline extracted/flux-calibrated spectra are subject to zero-point uncertainties that particularly affect sources with faint continua. Note that the EW sign convention is reversed, i.e. a positive EW value means net emission.

| | IPHAS name/position | IPHAS photometry | | | 2MASS magnitudes | | | H$\alpha$(EW) |
|---|---|---|---|---|---|---|---|---|
| | J[RA(2000)+Dec.(2000)] | $r'$ | $r' - i'$ | $r' - \mathrm{H}\alpha$ | $J$ | $H$ | $K$ | (Å) |
| C1 | J203228.09+414008.0 | 19.34 ± 0.02 | 1.64 ± 0.02 | 0.88 ± 0.04 | 14.66 ± 0.04 | 13.25 ± 0.03 | 12.55 ± 0.03 | 30 |
| C2 | J203432.58+413641.5 | 20.09 ± 0.03 | 1.71 ± 0.03 | 1.22 ± 0.05 | 15.91 ± 0.07 | 14.63 ± 0.05 | 14.47 ± 0.10 | 100 |
| C3 | J203258.80+413209.6 | 19.12 ± 0.02 | 1.70 ± 0.02 | 1.14 ± 0.03 | 14.28 ± 0.03 | 12.90 ± 0.03 | 12.12 ± 0.02 | 70 |
| C4 | J203200.95+413114.0 | 19.70 ± 0.02 | 1.60 ± 0.02 | 0.92 ± 0.03 | 15.35 ± 0.05 | 14.10 ± 0.04 | 13.66 ± 0.05 | 70 |
| C5 | J203105.70+412834.7 | 20.30 ± 0.04 | 1.73 ± 0.05 | 1.37 ± 0.06 | 15.16 ± 0.05 | 13.69 ± 0.030 | 12.74 ± 0.03 | 105 |
| C6 | J203113.63+412744.1 | 18.40 ± 0.01 | 2.06 ± 0.01 | 1.10 ± 0.02 | 12.75 ± 0.02 | 11.40 ± 0.01 | 10.21 ± 0.02 | 60 |
| C7 | J203224.94+412521.0 | 19.77 ± 0.03 | 1.57 ± 0.02 | 0.85 ± 0.04 | 15.31 ± 0.04 | 13.91 ± 0.03 | 13.00 ± 0.03 | 50 |
| C8 | J203219.50+412337.6 | 21.05 ± 0.07 | 1.15 ± 0.05 | 1.62 ± 0.06 | >16.23 | 15.71 ± 0.13 | >14.36 | 250 |
| C9 | J203245.99+411042.6 | 19.72 ± 0.03 | 2.19 ± 0.04 | 0.86 ± 0.04 | 13.53 ± 0.04 | 12.00 ± 0.04 | >11.00 | 15 |
| C10 | J203217.27+410225.6 | 19.31 ± 0.02 | 1.40 ± 0.03 | 1.52 ± 0.03 | 15.56 ± 0.06 | 14.53 ± 0.07 | 14.38 ± 0.10 | 180 |

**Table 3.** Positions and magnitudes for the emission-line stars in Field S.

| | IPHAS name/position | IPHAS photometry | | | 2MASS magnitudes | | | H$\alpha$ EW |
|---|---|---|---|---|---|---|---|---|
| | J[RA(2000)+Dec.(2000)] | $r'$ | $r' - i'$ | $r' - \mathrm{H}\alpha$ | $J$ | $H$ | $K$ | (Å) |
| Objects not clustered near DR 15 | | | | | | | | |
| S1 | J203317.17+410015.5 | 19.85 ± 0.03 | 2.20 ± 0.04 | 1.07 ± 0.05 | 13.97 ± 0.05 | 12.51 ± 0.04 | 11.68 ± 0.03 | 30 |
| S2 | J203124.76+405944.3 | 20.30 ± 0.04 | 1.97 ± 0.05 | 1.32 ± 0.06 | 14.77 ± 0.04 | 13.26 ± 0.03 | 12.22 ± 0.02 | 120: |
| S3 | J203310.18+405903.7 | 18.16 ± 0.01 | 1.89 ± 0.01 | 0.79 ± 0.02 | 13.05 ± 0.02 | 11.72 ± 0.02 | 10.78 ± 0.02 | 12 |
| S4 | J203353.44+405449.1 | 18.78 ± 0.01 | 1.96 ± 0.01 | 1.46 ± 0.02 | 13.04 ± 0.02 | 11.70 ± 0.02 | 10.86 ± 0.01 | 125: |
| S5 | J203132.56+405138.5 | 20.34 ± 0.05 | 1.80 ± 0.06 | 1.25 ± 0.07 | 16.16: | 14.58 ± 0.06 | 14.11 ± 0.07 | 70 |
| S6 | J203043.02+405033.6 | 19.62 ± 0.02 | 1.89 ± 0.02 | 1.24 ± 0.04 | 15.85 ± 0.07 | 15.22 ± 0.09 | 14.90 ± 0.14 | 80 |
| S7 | J203123.14+405024.9 | 18.00 ± 0.01 | 1.61 ± 0.01 | 0.74 ± 0.02 | 13.47 ± 0.03 | 12.32 ± 0.03 | 11.64 ± 0.02 | 20 |
| S8 | J203314.89+404909.8 | 20.37 ± 0.05 | 2.24 ± 0.05 | 1.27 ± 0.07 | 14.48 ± 0.03 | 13.07 ± 0.02 | 12.26 ± 0.02 | 70 |
| S9 | J203253.33+404823.7 | 17.54 ± 0.01 | 1.68 ± 0.01 | 0.61 ± 0.01 | 12.82 ± 0.02 | 11.49 ± 0.02 | 10.40 ± 0.02 | 20 |
| S10 | J203101.33+404200.7 | 19.75 ± 0.03 | 1.73 ± 0.04 | 1.15 ± 0.04 | 15.00 ± 0.05 | >13.55 | >12.764 | 110: |
| S11 | J203206.86+403952.8 | 19.56 ± 0.02 | 2.10 ± 0.03 | 0.90 ± 0.04 | 14.04 ± 0.03 | 12.72 ± 0.03 | 11.92 ± 0.02 | 20 |
| S12 | J203125.87+403231.8 | 19.58 ± 0.03 | 2.04 ± 0.03 | 0.92 ± 0.04 | 14.37 ± 0.03 | 13.23 ± 0.03 | 12.81 ± 0.03 | 20 |
| S13 | J203347.69+402547.1 | 19.07 ± 0.02 | 2.43 ± 0.02 | 1.02 ± 0.03 | 12.67 ± 0.03 | 11.50 ± 0.02 | 10.68 ± 0.02 | 40 |
| Objects located in the vicinity of DR 15 | | | | | | | | |
| S14 | J203150.28+402333.1 | 20.32 ± 0.05 | 1.98 ± 0.06 | 1.12 ± 0.07 | 14.93 ± 0.04 | 13.57 ± 0.03 | 12.99 ± 0.03 | 60 |
| S15 | J203209.72+402253.6 | 18.91 ± 0.01 | 1.88 ± 0.02 | 1.11 ± 0.02 | – | – | – | 60 |
| S16 | J203155.32+402216.8 | 19.96 ± 0.03 | 1.99 ± 0.04 | 1.34 ± 0.04 | 14.66 ± 0.03 | 13.22 ± 0.03 | 12.43 ± 0.02 | 90 |
| S17 | J203151.67+402128.6 | 19.89 ± 0.03 | 2.22 ± 0.03 | 0.89 ± 0.05 | 14.08 ± 0.03 | 12.52 ± 0.02 | 11.66 ± 0.02 | 15 |
| S18 | J203248.51+402105.0 | 17.69 ± 0.01 | 1.55 ± 0.01 | 1.22 ± 0.01 | 13.91 ± 0.02 | 12.83 ± 0.02 | 12.10 ± 0.022 | 100: |
| S19 | J203113.61+402013.0 | 20.12 ± 0.04 | 2.26 ± 0.04 | 1.04 ± 0.06 | 14.09 ± 0.03 | 12.51 ± 0.02 | 11.73 ± 0.02 | 20 |
| S20 | J203234.88+401811.1 | 17.01 ± 0.00 | 1.25 ± 0.01 | 0.91 ± 0.01 | 13.59 ± 0.02 | 12.53 ± 0.02 | 11.90 ± 0.02 | 20 |
| S21 | J203300.81+401800.4 | 17.53 ± 0.01 | 1.23 ± 0.01 | 1.76 ± 0.01 | 14.21 ± 0.03 | 13.17 ± 0.03 | 12.62 ± 0.03 | 200: |
| S22 | J203220.50+401755.7 | 19.62 ± 0.02 | 2.00 ± 0.03 | 0.95 ± 0.04 | 14.91 ± 0.05 | 13.70 ± 0.05 | 13.04 ± 0.04 | 20 |
| S23 | J203235.81+401745.1 | 18.45 ± 0.01 | 1.63 ± 0.01 | 0.69 ± 0.02 | 13.91: | 12.71 ± 0.03 | 12.11 ± 0.03 | 10 |
| S24 | J203017.09+401652.9 | 20.22 ± 0.04 | 2.22 ± 0.04 | 1.13 ± 0.06 | 12.68 ± 0.02 | 11.86 ± 0.02 | 11.56 ± 0.02 | 50 |
| S25 | J203159.07+401648.2 | 18.72 ± 0.01 | 1.83 ± 0.02 | 1.45 ± 0.02 | 14.48 ± 0.03 | 13.55 ± 0.02 | 13.13 ± 0.03 | 250: |
| S26 | J203207.81+401636.5 | 20.03 ± 0.03 | 1.98 ± 0.04 | 1.60 ± 0.04 | 15.19 ± 0.04 | 14.20 ± 0.04 | 13.62 ± 0.05 | 120: |
| S27 | J203232.72+401632.0 | 17.46 ± 0.01 | 1.41 ± 0.01 | 1.07 ± 0.01 | 13.82 ± 0.02 | 12.73 ± 0.02 | 12.11 ± 0.02 | 45 |
| S28 | J203200.66+401622.1 | 18.66 ± 0.01 | 1.78 ± 0.01 | 1.14 ± 0.02 | 14.37 ± 0.03 | 13.33 ± 0.03 | 12.80 ± 0.03 | 60 |
| S29 | J203255.04+401617.4 | 17.14 ± 0.01 | 1.25 ± 0.01 | 1.01 ± 0.01 | 13.47 ± 0.02 | 12.38 ± 0.02 | 11.68 ± 0.02 | 40 |
| S30 | J203146.62+401542.8 | 18.03 ± 0.01 | 1.41 ± 0.01 | 0.92 ± 0.01 | 14.35 ± 0.03 | 13.21 ± 0.03 | 12.60 ± 0.03 | 20 |
| S31 | J203229.79+401539.8 | 18.71 ± 0.01 | 2.05 ± 0.01 | 1.09 ± 0.02 | 14.22 ± 0.04 | 13.20 ± 0.04 | 12.79 ± 0.04 | 28 |
| S32 | J203149.02+401538.1 | 19.25 ± 0.02 | 1.53 ± 0.02 | 1.67 ± 0.02 | 15.30 ± 0.04 | 14.33 ± 0.05 | 13.90 ± 0.06 | 170: |
| S33 | J203301.12+401449.4 | 19.31 ± 0.02 | 1.35 ± 0.03 | 1.85 ± 0.02 | 14.98 ± 0.05 | 13.50 ± 0.04 | 12.49 ± 0.02 | 450: |
| S34 | J203306.07+401211.9 | 20.25 ± 0.04 | 2.33 ± 0.04 | 1.12 ± 0.05 | 15.27 ± 0.05 | 14.62 ± 0.06 | 14.36 ± 0.09 | 60 |
| S35 | J203339.55+401202.7 | 19.50 ± 0.02 | 2.23 ± 0.03 | 0.77 ± 0.04 | 13.60 ± 0.02 | 12.14 ± 0.02 | 11.21 ± 0.02 | 15 |
| S36 | J203309.80+401154.8 | 18.66 ± 0.01 | 1.56 ± 0.02 | 1.43 ± 0.02 | 14.72 ± 0.04 | 13.41 ± 0.03 | 12.53 ± 0.02 | 140 |
| S37 | J203215.98+401023.6 | 19.06 ± 0.01 | 1.74 ± 0.02 | 0.76 ± 0.02 | 14.80 ± 0.04 | 13.72 ± 0.03 | 13.08 ± 0.03 | 13 |
| S38 | J203336.84+400939.0 | 18.76 ± 0.01 | 2.02 ± 0.02 | 1.23 ± 0.02 | 13.92 ± 0.02 | 12.87 ± 0.02 | 12.33 ± 0.02 | 50 |

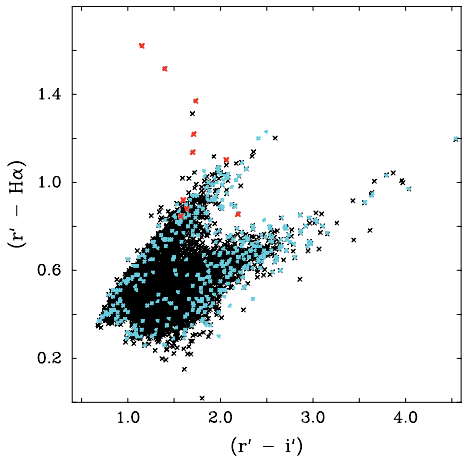


**Figure 2.** The colour–colour diagram used for the selection of HectoSpec targets in Field C. The dense locus of points plotted in black shows the IPHAS colours of all catalogued point sources, in the magnitude range $17 < r' < 20$, within 30 arcmin of the field centre. The blue data points are the colours of the objects for which we have HectoSpec data. In red, we pick out the objects with H$\alpha$ emission that are listed in Table 2.

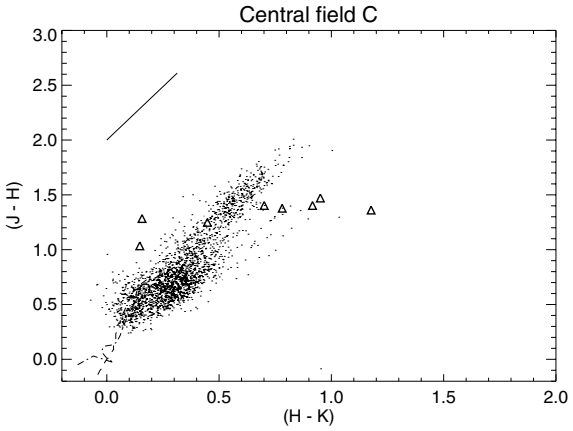


**Figure 3.** 2MASS data for IPHAS field 5985 (with $12 < J < 15$) and the strong H$\alpha$ emitting objects in the central Cyg OB2 Field C. The solid line in the top right-hand corner indicates the interstellar reddening line due to Bessell & Brett (1988). The dashed and dash–dotted lines in the bottom right-hand corner denote the main sequence for luminosity class V and III objects.

the better quality IPHAS imaging obtained in 2004 August. We also include $J$, $H$ and $K$ magnitudes from the Two Micron All Sky Survey (2MASS) data base, as these assist in constraining the nature of the line-emitting objects via their broad-band infrared (IR) colours. After presenting the data for Fields C and S, we discuss the clustering in the southern part of Field S in close proximity to DR 15 (Downes & Rinehart 1966), and on the LBV candidate G79, before briefly commenting on the six additional emission-line stars found in the eastern Fields Ea, Eb and Ec.

### 3.1 The centre of Cyg OB2: Field C

#### *3.1.1 Optical IPHAS photometry*

Fig. 2 presents the IPHAS colour–colour diagram for Field C, with the 10 H$\alpha$ emitting objects picked out in red. Note that sources C8 and C10 lie at the top of the IPHAS colour–colour diagram, as expected on the basis of their large measured H$\alpha$ EWs on either side of 200 Å (250 and 180 Å, respectively, Table 2). Similarly, the emission-line objects with the smallest H$\alpha$ EW (e.g. C1 and C9) tend to present lower $(r' - \mathrm{H}\alpha)$. Nevertheless, there is not a perfect correlation, since any of stellar H$\alpha$ variability, differences in the underlying spectral energy distribution, and residual uncertainties in the sky subtraction can obscure.

We further note that six of the 10 emission-line objects have $1.57 < (r' - i') < 1.73$ (C1, C2, C3, C4, C5, C7). C6 and C9 are even redder. If the intrinsic colours of these objects were to be like those of A and earlier type stars, their reddenings are likely to be $A_V \sim 7$ or more. This is easily within the range already known to be typical of Cyg OB2. Given the apparent brightness of these stars ($18.4 < r' < 20.3$), absolute magnitudes, $M(r')$ of $\sim$2, or brighter are implied for a distance modulus (DM) of 11.

On photometric grounds alone, we might conclude that these objects are classical Be stars within Cyg OB2, but when more evidence is taken into account, it is more plausible they are mainly in the PMS phase, as Herbig or T Tauri stars.

#### *3.1.2 Near-infrared 2MASS photometry*

In order to better pin down the character of the H$\alpha$ emitting objects, and to test for youth via the presence of accretion discs, we have examined NIR photometry from the 2MASS all-sky survey. A strong dusty NIR excess would distinguish the line-emitting objects from classical Be stars which fall in a different regime within the $(H - K)$ versus $(J - H)$ colour–colour diagram (e.g. see fig. 2 in Corradi, Rodriguez-Flores & Mampaso 2008).

Eight of the emission-line objects within Field C are plotted in the 2MASS $(J - H)$ versus $(H - K)$ colour–colour diagram in Fig. 3, along with point sources from IPHAS field 5985 (lying inside Field C). Objects C5, C6, C7 and (marginally) C3 are found to the right-hand side of the main locus of field stars and below the OB star reddening line, indicating an NIR excess. Such an excess can be a signature of a circumstellar disc around a young PMS T Tauri or Herbig Ae/Be star, although it only implies the *presence* of dust and it does not provide information on the circumstellar geometry, as NIR excesses may sometimes be due to (or confused with) IR companion stars (see e.g. Duchene et al. 2003 on V773 Tau).

Objects C4, C10, C2 and (marginally) C1 exhibit NIR colours associated with intrinsically red late-type objects within or above the reddened main-sequence band. C8 and C9 cannot be plotted in Fig. 3 because one or more of their *JHK* magnitudes is an upper limit.

#### *3.1.3 Optical spectroscopy with MMT/HectoSpec*

The final characterization of the discovered emission-line stars is essentially upheld by the optical HectoSpec data, in which we have looked for characterizing spectral indicators. Since the work of Hamann & Persson (1992a,b) it has been recognized that the Ca II IR triplet is a useful tool to identify T Tauri and Herbig Ae/Be stars, with about half of them showing it in emission. We show the best exposed representative examples, C6 and C10, in Fig. 4.

The NIR-excess objects, C3, C5 and C6 show the Ca II IR triplet in emission, with only C3 showing a hint of M star molecular bands. The non-excess objects C8 and C9 also show the triplet in emission, and share the apparently featureless continua of C5 and C6. C7 is

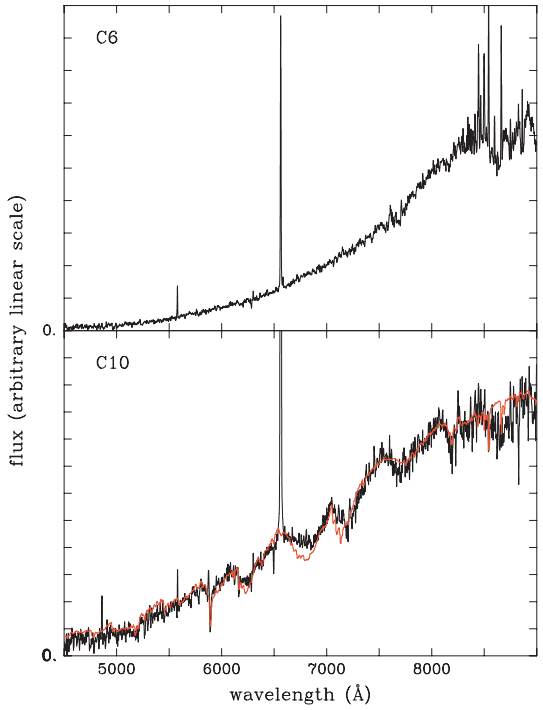


**Figure 4.** The spectra of C6 and C10. The data have been approximately flux calibrated, and the vertical scales are linear in both panels. C6, in the upper panel, is representative of five to six objects from Field C in presenting a significantly reddened, featureless continuum (at the modest S/N of the data): it is one of four in Field C to show the Ca II IR triplet in emission. Object C10, on the other hand, shows clearly the molecular bands typical of an M dwarf. Superimposed in red is the spectrum of an M2V star (Pickles 1998) reddened by 1.9 mag. Objects C1, C2 and C4 may be similar.

the only NIR-excess object in which the Ca II lines are not detected in emission: at the poor signal-to-noise ratio (S/N) achieved, its continuum is also apparently featureless.

In all of C1, C2, C4 and C10, there is evidence of the broad molecular bands typical of M stars. In the best exposed example, C10, these features are seen at greatest contrast. In this case, the spectrum can be dereddened, assuming $A_V$ is ∼2, to fit it acceptably well to the M2V spectrum in the Pickles (1998) library (see Fig. 4). The relatively low reddening needed for this, compared with the typical range for Cyg OB2, could indicate C10 is a foreground object. However, the combination of great H$\alpha$ EW and M2 spectral type identifies it as a T Tauri star (Barrado Navascues & Martin 2003). Hence it would be plausible to find C10 in or close to the main Cyg OB2 association at DM ∼ 11. At an $r'$ magnitude of 19.3, and for $A_V \sim 2$, a DM of 11 implies an absolute $M(r')$ magnitude of ∼6.5 for C10. Correcting this to $V$ for an early M star yields $V \sim 7.5$, which is around 3 mag brighter than expected for the early-M main sequence (Jahreiss & Wielen 1997). This is compatible with expectation for a T Tauri star (see e.g. Kenyon & Hartmann 1995).

No object in Table 2 has a bluer optical continuum than C10. Given how faint all these emission-line stars are, it would be more contrived to place any of them in the foreground than to adopt the working hypothesis that the bulk of these objects are PMS stars falling within Cyg OB2's sphere of influence at DM ∼11.

### 3.2 To the south of Cyg OB2: Field S

#### *3.2.1 The clustering linked to the DR 15 region*

From Fig. 1, it is very clear that around half of all the confirmed emission-line stars are concentrated within as little as a tenth of the observed sky area. Furthermore it can be seen that the H II region DR 15 is located in the midst of this grouping. Hence the first possibility to consider is that these emission-line stars belong to the same star-forming cloud as DR 15.

Balloon observations by Emerson, Jennings & Moorwood (1973) identified the H II region DR 15 (Downes & Rinehart 1966) to be an unresolved IR source with a total luminosity exceeding 20 000 $L_\odot$ for an assumed distance of 1 kpc (the most commonly quoted distance, due to Wendker et al. 1991). Subsequent NIR observations by Comeron & Torra (2001), Dutra & Bica (2001) and LeDuigou & Knödlseder (2002) reveal two separate structures with different reddenings and probably different distances. The centre of the cluster is found to be very close to both the DR 15 H II region and IRAS source 20306+4005 (Parthasarathy, Jain & Bhatt 1992). This IRAS source is also very close to our Field S source S31.

For the purpose of presenting the spectra of all the Field S sources, we divide them into two groups: the more northerly objects in the field, S1 to S13, are not viewed as candidate members of the DR 15 cluster, while S14 to S38 are treated as such. The dividing line between these two groups is at declination (Dec.) +40°24′.

#### *3.2.2 spectral classification of Field S objects*

Fig. 5 represents the IPHAS colour–colour diagram for the 38 line-emitting objects found in Field S. The photometry and measured H$\alpha$ EWs are set out in Table 3. Again, to better characterize the H$\alpha$ emitting objects and to test for youth, we examined NIR

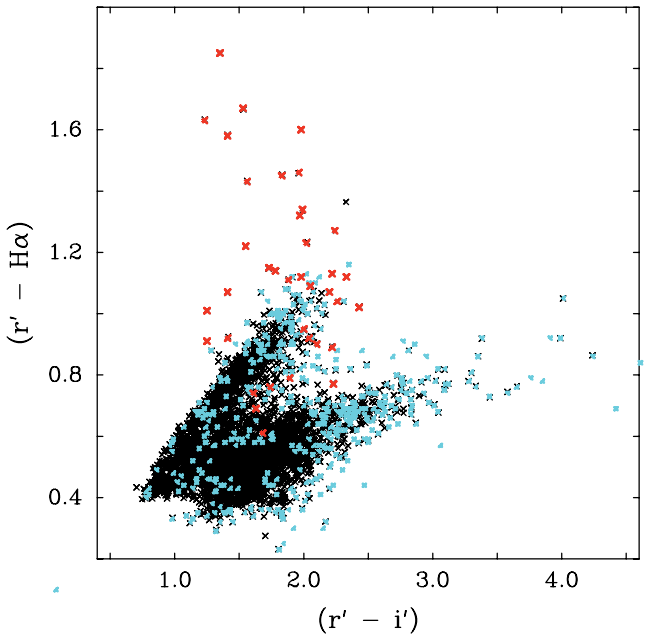


**Figure 5.** The colour–colour diagram used for the selection of HectoSpec targets in Field S. The dense locus of points plotted in black shows the IPHAS colours of all catalogued point sources, in the magnitude range $17 < r' < 20$, within 30 arcmin of the field centre. The blue data points are the colours of the objects for which we have HectoSpec data. In red, we pick out the objects with H$\alpha$ emission that are listed in Table 3.

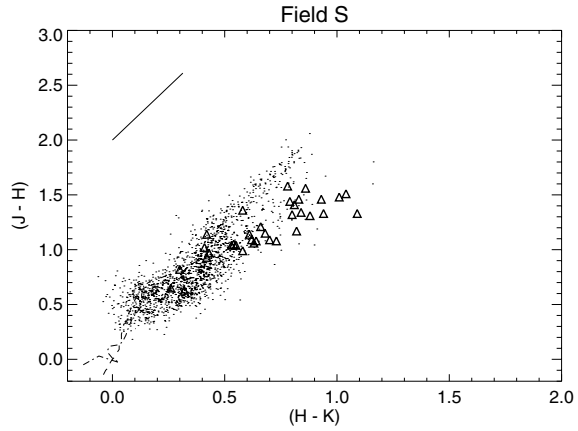


**Figure 6.** 2MASS data for IPHAS field 6010 (with $12 < J < 15$) and the strong H$\alpha$ emitting objects in Cyg OB2 Field S. The solid line in the top right-hand corner indicates the interstellar reddening line due to Bessell & Brett (1988). The dashed and dash–dotted lines in the bottom right-hand corner denote the main sequence for luminosity class V and III objects.

photometry from 2MASS. 35 of the 38 emission-line objects in Field S are plotted in the 2MASS ($J - H$) versus ($H - K$) colour–colour diagram in Fig. 6, along with point sources from IPHAS field 6010 (overlapping Field S). The large majority of objects are found in or to the right-hand side of the main locus of field stars. Clear NIR excesses are present in nine of them.

The two spatial groupings do not strongly separate in terms of their optical line emission characteristics (H$\alpha$ EW; Ca II triplet emission). The spectra of the 38 line-emitting objects in Field S were generally of higher quality than those in the central Field C, allowing more incisive evaluation. The Field S spectra were closely inspected and were divided into two spectroscopic groups: those presenting M-type molecular bands (Table 4), and those without them (Table 5) indicative of earlier spectral types. Three representative spectra, S6, S9 and S18 are plotted in Fig. 7.

Of the 16 objects from Field S showing M-type molecular bands, object S6 has been selected for illustration in Fig. 7 as it is one of the most easily typed of our discoveries. The spectrum is a reasonable match to M4V (Pickles 1998) and shows little sign of reddening. At the same time its strong H$\alpha$ emission (EW $\sim$80 Å) clearly signals youth. The type of M4 is the latest type to be assigned to any of our objects. If we require S6 to be closer than 1 (or 1.5 kpc), its absolute magnitude is fainter than $M_V \sim 8$ (or $\sim$7). Following the data given by Jahreiss & Wielen (1997), we would estimate $M_V \sim 12$ for an object already on the main sequence.

All objects in the M-type table satisfy the criteria based on spectral type and H$\alpha$ EW of Barrado Navascues & Martin (2003) that allow them to be designated classical T Tauri stars. Atomic line EWs are given in columns (2) and (3) of Table 4, whilst the characterizing molecule indices I1, I2 and I3 of Martin & Kun (1995) are given in columns (4)–(6). Note that, in some stars, the I3 index denominator is affected by He I emission at 6678 Å. The spectral type, derived from indices I1 to I3, is given in column (7), whilst the spectral type estimated from the appearance of the spectrum longward of 7000 Å is given in column (8). Where this second type is noticeably later than that implied by the indices I1–I3 from column (7), it is likely that significant continuum veiling is also present (see notes in column 9). All but two of the objects in Table 4 are located in the southern part of the field near to DR 15.

S9 is shown as an example of the Field S emission-line stars without evident molecular bands (Table 5). On the sky, these objects fall more evenly between the more northerly and DR 15 groups. F, G and K spectral types are most likely to apply to this selection, and many are likely to be young stars on account of their H$\alpha$ EWs, and the high frequency of Ca II IR-triplet emission (around half of the list). The spectrum of S9 could be sufficiently early in type to be described as a Herbig Ae star. The presence of atomic emission (columns 2–4, in Table 5) and absorption (columns 5 and 6)

**Table 4.** Spectroscopic properties of the Field S emission-line stars with M-type molecular bands. All these objects satisfy the criteria, using spectral type and H$\alpha$ EW (Barrado Navascues & Martin 2003), to be designated classical T Tauri stars. Where the spectral type estimated from comparing the appearance of the spectrum longward of 7000 Å is noticeably later than that consistent with the indices, I1–I3, it is an indication of significant continuum veiling.

| | EWs in Å | | Indices | | | Spectral type | | Veiled? | Comment |
|---|---|---|---|---|---|---|---|---|---|
| | [S II] 6717,6730 | Li I 6708 | I1 (CaH) | I2 (CaH) | I3 (TiO) | from I1, I2, I3 | >7000 Å | | |
| S4 | –,– | – | 1.09 | 1.29 | 0.94 | M0.5 ± 0.5 | ? | | |
| S6 | −7,−7 | – | 1.43 | 1.68 | 1.48 | M5 ± 1 | M4 | No | $E(B-V) \simeq 0$ |
| S18 | −1.4,−2.0 | – | 1.06 | 1.27 | 1.09 | M0 ± 0.5 | M2 | | Ca II IR triplet emission cf. DG Tau |
| S21 | –,– | 0.5 | 1.05 | 1.19 | 0.98 | K7/M0 | M0 | No | Ca II IR triplet emission |
| S22 | –,– | 0.4: | 1.12 | 1.29 | 1.08 | M0.5 ± 0.5 | M3 | Yes | |
| S24 | –,– | – | 1.23 | 1.48 | 1.49 | M3.5 ± 0.5 | M6 | Yes | |
| S25 | –,– | 0.2 | 1.15 | 1.31 | 1.21 | M1 ± 0.5 | M3 | | Ca II IR triplet emission |
| S26 | –,– | 0.5 | 1.17 | 1.40 | 1.24 | M1.5 ± 0.5 | M3 | | Ca II IR triplet emission |
| S27 | –,−0.4 | 0.4 | 1.06 | 1.14 | 0.98 | K7 ± 0.5 | M1 | Yes | Ca II IR triplet emission |
| S28 | –,– | 0.7 | 1.13 | 1.29 | 1.08 | M0.5 ± 0.5 | M2–M3 | | Ca II IR triplet emission |
| S30 | –,– | 0.5 | 1.07 | 1.17 | 1.00 | K7 ± 0.5 | M2 | Yes | |
| S31 | −0.6,−0.4 | 0.5 | 1.21 | 1.38 | 1.32 | M2 ± 0.5 | M4 | | |
| S32 | −0.4,−0.3 | 0.2 | 1.13 | 1.26 | 1.04 | M0.5 ± 0.5 | M3 | Yes | Ca II IR triplet emission |
| S34 | –,– | – | 1.25 | 1.50 | 1.35 | M3.5 ± 0.5 | M4 | No | $E(B-V) \simeq 0.6$ |
| S37 | –,– | 0.8 | 1.10 | 1.21 | 0.96 | M0 ± 0.5 | M0–M1 | No | $E(B-V) \simeq 1$ |
| S38 | –,– | 0.4 | 1.14 | 1.26 | 1.04 | M0.5 +/−0.5 | M2 | | Ca II IR triplet emission |

**Table 5.** Spectroscopic properties of the Field S emission-line stars without evident molecular bands (non-M type).

| | Emission features | | | Absorption features | | Spectral type | Comment |
|---|---|---|---|---|---|---|---|
| | He I | O I | Ca II | Li I | 6162,6495 | | |
| S1 | No | No | No | Yes? | No, yes | G/K? | |
| S2 | Yes | Yes | Yes | No | No, no | | |
| S3 | Yes | Yes | No | Yes | Yes, yes | | |
| S5 | | | | | | | Noisy |
| S7 | No | No | No | No | Yes, yes | K? | |
| S8 | No | Yes | Yes | ? | No, no | | |
| S9 | Yes | No | No | No | No, yes? | Ae | $E(B-V) \simeq 2.3$ |
| S10 | Yes | Yes | Yes | No | Yes, yes | G/K | |
| S11 | No | Yes | No | No | No, no | | |
| S12 | No | No | No | No | No, yes | K? | |
| S13 | No | Yes | Yes | No | No, no | | $E(B-V) \sim 3.5$ |
| S14 | No | | No | | | G/K | |
| S15 | Yes | | Yes | No | Yes, yes | G/K | |
| S16 | Yes | Yes | Yes | No | Yes, no | | |
| S17 | No | No | No | No | Yes, yes | K? | |
| S19 | No | No | No | No | Yes, yes | G/K | |
| S20 | No | No | No | Yes | Yes, yes | K | |
| S23 | No | No | No | Yes | Yes, yes | G? | |
| S29 | Yes | Yes | Yes | Yes? | Yes/yes | K | |
| S33 | Yes | Yes | Yes | No | | | |
| S35 | No | No? | Yes? | | No, yes | G/K? | |
| S36 | Yes | Yes | Yes | No | Yes, no | | |

features is used, where possible, to roughly appraise spectral type (column 7).

Finally, we present the spectrum of object S18 (bottom panel of Fig 7). It shows molecular bands that are typical of an M dwarf. The Ca II IR emission lines are spectacularly strong. Even with the 6.2-Å resolution of the HectoSpec spectra their peak fluxes are almost ten times the continuum level. Unusually, S18 also shows a very rich array of further low-excitation atomic emission lines in its spectrum – a property it shares with the well-known T Tauri star, DG Tau (see Hessman & Guenther 1997).

### *3.2.3 The status of the LBV candidate G79.29+0.46*

The LBV candidate (LBVc) G79.29+0.46 was discovered as a ring-like radio source by Higgs, Wendker & Landecker (1994). In a recent study examining the location of LBVs in the Hertzsprung–Russell diagram, Smith, Vink & de Koter (2004) positioned the LBV candidate G79 at an absolute magnitude of $\log L/L_{\odot} = 6.1$ for an assumed distance of 1.7 kpc. Above, we discussed the possibility that the southern clustering of emission-line objects may be associated with the DR 15 region rather than with Cyg OB2 itself. Given that – on the sky – G79 is extremely close to the discovered line-emitting objects, we may wish to revisit the distance and luminosity of G79. If G79 would be a PMS belonging to the same group of stars that appears to be associated with DR 15, its distance may need to be revised downward to $\sim$1 kpc and its intrinsic luminosity would drop to about $\log L/L_{\odot} = 5.65$. Although this may have consequences for its position on the S Dor instability strip in the Hertzsprung–Russell diagram (see fig. 1 in Smith et al. 2004), its luminosity would still be in line with that of an evolved massive star rather than that of an intermediate mass PMS. In other words, we keep G79 in the list of LBV candidates.

For any evolved star to officially classify as an LBV (i.e. to drop the 'c' from LBVc), the object needs to be subject to significant spectral and photometric variations (of more than 1 mag) on the time-scale of years to decades (e.g. Humphreys & Davidson 1994). This is a relevant issue, as the total number of Galactic LBVs is only of the order of 5–10. Given that IPHAS revisited the field of CygOB2 on a number of occasions over the period 2003–2005, this may enable us to obtain vital information on G79's evolutionary status, either confirming or eliminating it as a bona fide LBV.

The IPHAS $r'$ magnitude ($r' = 14.91$, measured Oct 16 2003) has not shown enough variability over the 2003–2005 period for G79 to be officially added to the LBV class. Monitoring over longer time-scale is required. Potential $(r' - i')$ colour variability (note that $r' - i' = 2.92$ on 2003 October 16) could be caused by temperature and/or mass-loss variations. For the sake of completeness and future reference, we quote G79's UV magnitude of $U = 19.744 \pm 0.035$ (from UVEX data taken on 2006 June 27) and its NIR photometry from 2MASS with $J = 6.91(\pm\ 0.02), H = 5.29(\pm\ 0.02)$ and $K = 4.33(\pm\ 0.01)$.

More significantly, we can report IPHAS variable line emission, as $(r' - \mathrm{H}\alpha)$ varied from 1.05 on 2003 October 16, up to $(r' - \mathrm{H}\alpha) = 1.41$ (on 2004 August 9), and returning to $(r' - \mathrm{H}\alpha) = 1.08$ on 2005 November 1. This excursion suggests the occurrence of changes in the mass-loss rate causing the H$\alpha$ EW variability. Previously, Voors et al. (2000) studied the spectrum of G79 and found the H$\alpha$ EW to be $\simeq$50 Å. Our line-emission variability, underlying the IPHAS $(r' - \mathrm{H}\alpha)$ changes, indicates line EW changes by several tens to hundreds of angstroms (see fig. 6 in Drew et al. 2005), corresponding to EW changes by a factor of 2 or more. This kind of H$\alpha$ EW variability is not extraordinary in comparison to bona fide Galactic LBVs, such as AG Car, whose H$\alpha$ EW varied from $\sim$50 to $\sim$200 Å within a few years (Stahl et al. 2001). This is in line with predicted LBV mass-loss variability due to changes in the ionization of Fe that drives the winds of LBVs (Vink & de Koter 2002).

Although we do not have definitive proof that G79 is a true LBV, all available evidence points in this direction. This assertion

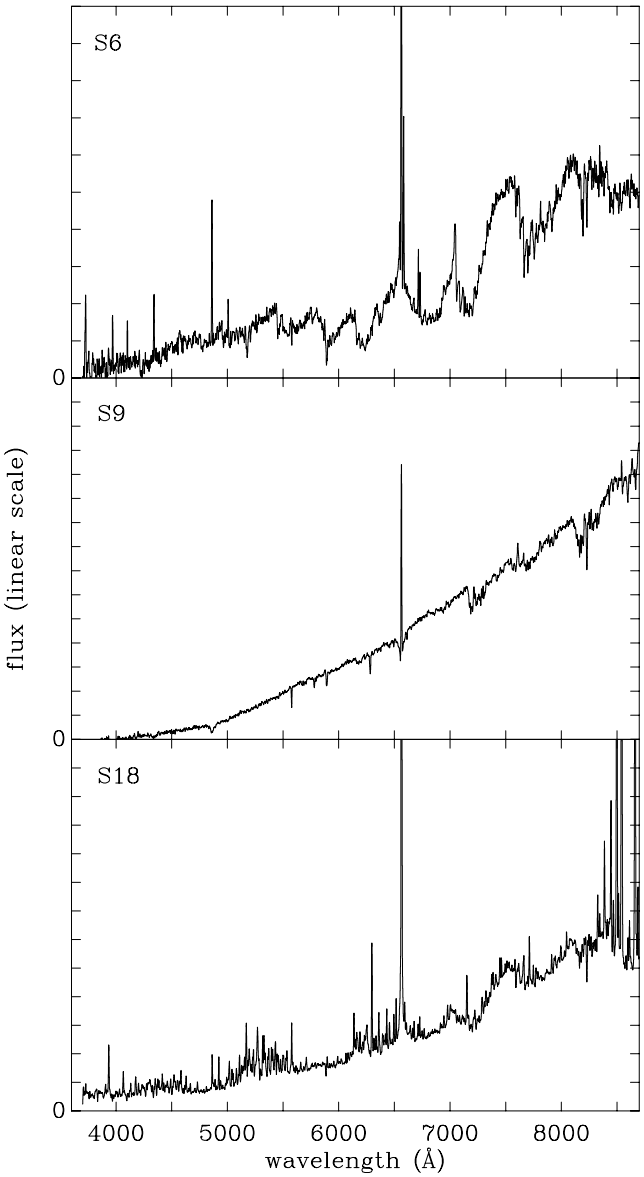


**Figure 7.** The spectra of S6, S9 and S18. The data have been approximately flux calibrated, and the vertical scales are linear in all three panels. S6 is representative of 16 objects from Field S in showing M-type molecular bands. S9 is more representative of the Field S emission-line stars without evident molecular bands. These are F/G/K T Tauri stars, while the spectrum of S9 itself is more characteristic of a Herbig Ae star. Object S18 shows the molecular bands typical of an M dwarf, and shows the Ca II IR triplet strongly in emission. It has a strong H$\alpha$ line and the rich emission-line spectrum is reminiscent of that of DG Tau.

strengthens even further when secondary indicators, such as the presence and morphological similarity of G79's circumstellar nebula to nebulae from confirmed LBVs such as AG Car are taken into account.

### 3.3 Fields Ea, Eb and Ec

Pointings Ea, Eb and Ec revealed six further strong H$\alpha$ emitting objects. All of these are found far above the unreddened main sequence, and their $(r' - i')$ colours, $\gtrsim$1.5, are in good agreement with the known range in reddenings for the environs of Cyg OB2. As can also be noted from Table 6, all objects in these fields show large NIR excesses, except for Ec1. Although sources Eb1 and Eb3 show the characteristic Ca II IR triplet strongly in emission, source Eb2 – despite exhibiting a larger NIR excess than source Eb3 – does not. We note that the extreme emission-line star Ec1, with an H$\alpha$ EW of 210 Å does not show a particularly large NIR excess. Object Ec2 stands out for its combination of 'moderate' H$\alpha$ EW of 59 Å, its relatively extreme NIR excess, and strong Ca II emission.

## 4 DISCUSSION

### 4.1 The nature of the H$\alpha$ emitters

On the basis of photometric survey data and highly efficient fibre spectroscopy as follow-up, we have discovered over 50 strong H$\alpha$ emitting objects towards the large OB association Cyg OB2 and the neighbouring H II region DR 15. The greater concentration of our discoveries – nearly half of them – lies in an arc adjacent to the latter.

Ca II IR triplet emission is clearly seen in the spectra of 26 out of 54 emission-line objects. A similar fraction shows a dusty NIR excess that distinguishes them from classical Be stars. In many of the M-type discoveries the H$\alpha$ EW is clearly too extreme to allow them to be classified simply as active main-sequence objects. Taking these properties altogether, it seems likely that the bulk of our sample consists of objects in their PMS phase of evolution.

But how massive are these objects, and how do the more scattered Cyg OB2 group and the more concentrated DR 15 group compare? To begin answering these questions, we would ideally assign reasonably precise spectral subtypes to the objects, but the combination of limited spectral resolution ($\sim$6 Å), together with the complicating attributes of continuum veiling and NIR excesses, prevent this at the present time. For the time being we therefore adopt a qualitative approach based on typical magnitudes, likely distances, and reddenings.

After a review of the literature on the distance of Cyg OB2 (Massey & Thompson 1991; Torres-Dodgen, Carroll & Tapia 1991; Hanson 2003), we have adopted a DM of 11.0 towards the region. The typical interstellar reddening into Cyg OB2 is commensurate with $E(B - V) \simeq 2$ (Massey & Thompson 1991; Albacete Colombo et al. 2007). Using the standard factor of $R_V = 3.1$ to convert $E(B - V)$ to visual extinction, we arrive at $A_V \simeq 6$–7 (or $A_{r'} \simeq 5$). Taking the observed IPHAS magnitudes, $18 < r' < 20$, for sources in Field C and the north of Field S, together with the DM ($\simeq 11$) and the typical reddening, the absolute $M(r')$ magnitudes can be deduced to fall in the range 2–4. On the main sequence, this magnitude range would correspond to late A and F spectral types. But some of our discoveries are less reddened M-type objects (e.g. the object C10 discussed in Section 3.1.3), which cannot be so intrinsically bright – even at the distance of Cyg OB2. The impression to emerge from this is that a mixture of Herbig and T Tauri stars has been uncovered.

The sources lying in the vicinity of DR 15 may be less distant (if we apply the reported figure of 1 kpc due to Wendker et al. 1991), perhaps somewhat brighter ($17 < r' < 20$), and possibly less reddened on the whole [$E(B - V) \sim 1$ may be typical]. The absolute magnitudes here are likely to fall in the range $6 < M_{r'} < 9$ – a somewhat fainter range than for the scattered Cyg OB2 candidate young stars in the more northern areas. This picture would be consistent with the appreciably higher fraction of DR 15 associated candidate objects presenting M-type spectra (around half, compared with one quarter for the more northern objects).

**Table 6.** Positions and magnitudes for the emission-line stars in Fields Ea, Eb and Ec.

| | IPHAS name/position | IPHAS photometry | | | 2MASS magnitudes | | | H$\alpha$ EW |
|---|---|---|---|---|---|---|---|---|
| | J[RA(2000)+Dec.(2000)] | $r'$ | $r'-i'$ | $r'-$H$\alpha$ | $J$ | $H$ | $K$ | (Å) |
| Ea1 | J203839.90+420118.2 | $19.83 \pm 0.02$ | $1.99 \pm 0.02$ | $1.48 \pm 0.04$ | $14.223 \pm 0.03$ | $12.760 \pm 0.03$ | $11.814 \pm 0.02$ | 111 |
| Eb1 | J204059.02+411051.9 | $18.017 \pm 0.01$ | $1.76 \pm 0.01$ | $1.40 \pm 0.01$ | $12.927 \pm 0.02$ | $11.174 \pm 0.02$ | $9.749 \pm 0.01$ | 210 |
| Eb2 | J204121.02+411721.6 | $18.952 \pm 0.01$ | $1.51 \pm 0.01$ | $1.60 \pm 0.01$ | $15.552 \pm 0.05$ | $13.868 \pm 0.04$ | $12.736 \pm 0.03$ | 102 |
| Eb3 | J204140.09+411228.1 | $17.390 \pm 0.01$ | $1.64 \pm 0.01$ | $1.39 \pm 0.01$ | $12.818 \pm 0.02$ | $11.431 \pm 0.02$ | $10.462 \pm 0.01$ | 89 |
| Ec1 | J204733.98+413137.0 | $18.162 \pm 0.02$ | $1.33 \pm 0.01$ | $1.64 \pm 0.01$ | $14.924 \pm 0.04$ | $14.088 \pm 0.04$ | $13.576 \pm 0.05$ | 210 |
| Ec2 | J204645.49+410700.0 | $18.532 \pm 0.02$ | $1.05 \pm 0.02$ | $1.23 \pm 0.01$ | $15.614 \pm 0.05$ | $14.222 \pm 0.04$ | $13.030 \pm 0.03$ | 59 |

Rather than objects in the foreground or unrelated to Cyg OB2, we expect the majority of objects to be directly associated with Cyg OB2 and DR 15.

### 4.2 Comments on diagnosing environmental influences on the newly revealed young stellar population

We draw attention to our discovery of line-emitting objects in the central portion of Cyg OB2. The presence of some disc accretors in potentially close proximity to massive OB stars may be considered significant, as the effect of UV photoevaporation of young discs – clearly operative on Orion's proplyds (O'dell et al. 1993) – seems well established. Nevertheless, we have revealed PMS objects towards CygOB2 that are embedded in circumstellar discs and which appear to be indistinguishable from the clustered objects towards the southern portion of the field. If the central OB stars have a pronounced effect on the evolution of PMS circumstellar discs, we might expect to witness a decreasing influence of OB stars when going from Field C PMS to the northern areas of Field S and to the area of clustered objects in the south (see the discussions in Guarcello et al. 2007; Mayne, Naylor & Littlefair 2007). However, there is no evidence for such a trend in the proportion of NIR excesses, or in the emission-line characteristics (e.g. presence/absence of the Ca II IR triplet and in the strength of the H$\alpha$ emission).

One possibility that was discussed above is that the objects clustering towards the south are closer to us than the objects in the north, and in this case there is no particular reason to search for trends. This would still not explain the presence of circumstellar discs in the central regions of Cyg OB2 in its own right. The mere existence of these discs could imply that the influence of OB stars on protoplanetary disc evolution has been exaggerated or that additional effects may hide the photoevaporation effect. Such a situation could be true if the central objects are on average more reddened. If these central PMS stars are still embedded in large amounts of molecular gas, this material may shield the discs from UV radiation more effectively, potentially compensating for the effect of their smaller separation from the UV emitters. Another option would be that the Field C PMS stars are younger, and the OB stars have simply not yet had enough time to evaporate the protoplanetary discs.

Alternatively we might just be at the beginning of finding candidate PMS objects across the face of Cyg OB2. The reason being that we might have expected to find many more young stars in a population no more than a few million years old, which is as rich in massive OB stars as this region, unless the majority of PMS consists of weak-lined T Tauri stars which are harder to pick out from their H$\alpha$ emission than classical T Tauri stars. Albacete-Colombo et al. (2007) studied the central regions of Cyg OB2 at X-ray wavelengths and found a low fraction (of only 4.4 per cent) of disc-induced NIR excesses. So far, the list of candidate young stars towards the centre of Cyg OB2 is as long as it is towards the more modest DR 15 region. A comparison in typical absolute magnitude of candidates between the two regions may hint that the limiting $r'$ magnitude of $\sim$20 may need to be increased to $\sim$23 or more in order to uncover the main young low-mass population in the centre. The encouraging lesson of this study is that insight into the star-forming environment within Cyg OB2 can be gained via photometry alone, given the high proportion of IPHAS candidate emission-line stars that are confirmed spectroscopically. A deeper targeted optical photometric study, incorporating narrow-band H$\alpha$ observations that was appropriately paired with NIR data may go a long way to resolving these issues.

A final possibility worthy of mention is that the PMS we have discovered towards the centre of CygOB2 are in reality somewhat in the near foreground of Cyg OB2. In other words, the central PMS could geometrically be at the same distance from the Cyg OB2 OB population as those we find in the southern area of Field S, near DR 15. For this concept to work the distances to the two groups of stars would need to be very similar. This is not ruled out given the continuing controversy over the distance to Cyg OB2 and its surroundings (e.g. placing everything at $\sim$1.4 kpc is a currently available option – see Hanson 2003) and a recent CO view of the Cygnus X region (Schneider et al. 2006). Note that 1° on the sky at a distance of 1–2 kpc corresponds to a length of 15–30 pc. The main difficulty would be to explain why reddenings across the face of Cyg OB2 may be higher than at the 'limb' (in this picture) in the vicinity of DR 15. This difference would indeed suggest that Cyg OB2 is distinct and more distant. If however this were not a problem, then the PMS objects presented here might all be seen as the consequence of triggered star formation on the periphery of the main OB association. If stellar winds and early supernovae in the centre of the association would have been responsible for this, the relevant time-scale is easily short enough to allow for this connection, as expansion at a sound speed of $10\,\mathrm{km\,s^{-1}}$ would take $\sim$3 Myr to travel $\sim$30 pc – a time-scale compatible with the age of Cyg OB2.

## ACKNOWLEDGMENTS

We would like to thank the MMT/HectoSpec team and the Isaac Newton Group for their assistance. This paper makes use of data from the Isaac Newton Telescope, operated on the island of La Palma by the Isaac Newton Group in the Spanish Observatorio del Roque de los Muchachos of the Instituto de Astrofisica de Canarias. The multi-object spectroscopic observations reported here were obtained at the MMT Observatory, a joint facility of the Smithsonian Institution and the University of Arizona. We acknowledge use of data products from the 2MASS, which is a joint project of the

University of Massachusetts and the Infrared Processing and Analysis Center/California Institute of Technology (funded by the USA's National Aeronautics and Space Administration and National Science Foundation). DS acknowledges a STFC Advanced Fellowship as well as support through the NASA guest observer programme. NJW acknowledges an STFC funded student fellowship.

## REFERENCES

Albacete Colombo J. F., Flaccomio E., Micela G., Sciortino S., Damiani F., 2007, A&A, 464, 211
Arias J. I., Barba R. H., Morrell N. I., 2007, MNRAS, 374, 1253
Barrado Navascues D., Martin E. L., 2003, AJ, 126, 2997
Bastian N., Gieles M., Lamers H. J. G. L. M., Scheepmaker R. A., de Grijs R., 2005, A&A, 431, 905
Bessell M. S., Brett J. M., 1988, PASP, 100 1134
Clark J. S., Negueruela I., Crowther P. A., Goodwin S. P., 2005, A&A, 434, 949
Comeron F., Torra J., 2001, A&A, 375, 539
Comeron F., Fernandez M., Baraffe I., 2003, A&A, 406, 1001
Corradi R. L. M., Rodriguez-Flores E. R., Mampaso A., 2008, A&A, 480, 409
Downes R., Rinehart R., 1966, ApJ, 144, 937
Drew J. E. et al., 2005, MNRAS, 362, 753
Duchene G., Ghez A. M., McCabe C., Weinberger A. J., 2003, ApJ, 592, 288
Dutra C. M., Bica E., 2001, A&A, 376, 434
Emerson J. P., Jennings R. E., Moorwood A. F. M., 1973, ApJ, 184, 401
Fabricant D. et al., 2005, PASP, 117, 1411
Figer D. F., McLean I. S., Morris M., 1999, ApJ, 514, 202
Gonzalez-Solares E. A. et al., 2008, preprint (arXiv:0712.0384)
Guarcello M. G., Prisinzano L., Micela G., Damiani F., Peres G., Sciortino S., 2007, A&A, 462, 245
Hamann F., Persson S. E., 1992a, ApJS, 82, 247
Hamann F., Persson S. E., 1992b, ApJS, 82, 285
Hanson M. M., 2003, ApJ, 597, 957
Herbig G. H., Dahm S. E., 2001, PASP, 113, 195
Hessman F. V., Guenther E. W., 1997, A&A, 321, 497
Higgs L. A., Wendker H. J., Landecker T. L., 1994, A&A, 291, 295
Humphreys R. M., Davidson K., 1994, PASP, 106, 1025
Jahreiss H., Wielen R., 1997, in Battrick B., Perryman M. A. C., Bernacca P. L., eds, ESA SP-402, HIPPARCOS'97: Presentation of the Hipparchos and Tycho Catalogues and First Astrophysical Results of the Hipparcos Space Astrometry Mission. ESA, Noordwijk, p. 675
Kenyon S. J., Hartmann L., 1995, ApJS, 101, 117
Knödlseder J., 2000, A&A, 360, 539
LeDuigou J.-M., Knödlseder J., 2002, A&A, 392, 869
Martin E., Kun M., 1995, A&AS, 116, 467
Massey P., Thompson A. B., 1991, AJ, 101, 1408
Mayne N. J., Naylor T., Littlefair S. P., 2007, MNRAS, 375, 1220
O'dell C. R., Wen Z., Hu X., 1993, ApJ, 410, 696
Odenwald S. F., Schwartz P. R., 1993, ApJ, 405, 706
Odenwald S. F., Campbell M. F., Shivanandan K., Schwartz P., Fazio G. G., Moseley H., 1990, AJ, 99, 288
Parthasarathy M., Jain S. K., Bhatt H. C., 1992, A&A, 266, 202
Pickles A. J., 1998, PASP, 110, 863
Pozzo M., Naylor T., Jeffries R. D., Drew J. E., 2003, MNRAS, 341, 805
Reddish V. C., Lawrence L. C., Pratt N. M., 1966, Publ. R. Obser. Edinburgh, 5, 111
Robberto M., Song J., Mora Carrillo G., Beckwith S. V. W., Makidon R. B., Panagia N., 2004, ApJ, 606, 952
Schneider N., Bontemps S., Simon R., Jakob H., Motte F., Miller M., Kramer C., Stutzki J., 2006, A&A, 458, 855
Smith L., Gallagher J. S., 2001, MNRAS, 326, 1027
Smith N., Vink J. S., de Koter A., 2004, ApJ, 615, 475
Stahl O., Jankovics I., Kovacs J., Wolf B., Schmutz W., Kaufer A., Rivinius Th., Szeifert Th., 2001, A&A, 375, 54
Stolte A., Brandner W., Brandl B., Zinnecker H., 2006, AJ, 132, 253
Torres-Dodgen A. V., Carroll M., Tapia M., 1991, MNRAS, 249, 1
Vink J. S., de Koter A., 2002, A&A, 393, 543
Voors R. H. M., Geballe T. R., Waters L. B. F. M., Najarro F., Lamers H. J. G. L. M., 2000, A&A, 362, 236
Wendker H. J., 1984, A&AS, 58, 291
Wendker H. J., Higgs L. A., Landecker T. L., 1991, A&A, 241, 551

This paper has been typeset from a TEX/LATEX file prepared by the author.